THE JOURNAL OF PHYSICAL CHEMISTRY C

Article

pubs.acs.org/JPCC

# Two-Dimensional Transition Metal Dichalcogenide Enhanced Phase-Sensitive Plasmonic Biosensors: Theoretical Insight

Qingling Ouyang,[†,§,▽] Shuwen Zeng,[†,§,▽] Li Jiang,[†,§,∥] Junle Qu,[*,‡] Xuan-Quyen Dinh,[§] Jun Qian,[∥] Sailing He,[∥] Philippe Coquet,[§,⊥] and Ken-Tye Yong[*,†,§]

[†]School of Electrical and Electronic Engineering, Nanyang Technological University, Singapore, 639798

[‡]Key Laboratory of Optoelectronics Devices and Systems of Ministry of Education/Guangdong Province, College of Optoelectronic Engineering, Shenzhen University, Shenzhen 518060, China

[§]CINTRA CNRS/NTU/THALES, UMI 3288, Research Techno Plaza, 50 Nanyang Drive, Border X Block, Singapore, 637553

[∥]State Key Laboratory of Modern Optical Instrumentation, Centre for Optical and Electromagnetics Research, Zhejiang University, Hangzhou 310058, China

[⊥]Institut d'Electronique, de Microélectronique et de Nanotechnologie (IEMN), CNRS UMR 8520−Université de Lille 1, 59650 Villeneuve d'Ascq, France

Supporting Information

**ABSTRACT:** Atomically thin transition metal dichalcogenide nanomaterials have shown superior optical and electronic properties in the two-dimensional (2D) scale. They are considered as promising alternative materials to graphene. Here, we have precisely engineered a plasmonic sensing substrate with four types of two-dimensional transition metal dichalcogenide nanomaterial to achieve significant phase sensitivity improvement. Phase modulation is currently the most sensitive interrogation method among all the plasmonic detection approaches. The tuning of the substrate thickness in an atomic scale with a step less than 1 nm allows the efficient modulation of phase signals. More importantly, the optical absorption rate for each of these nanomaterials is different and can be tuned by changing the number of 2D layers, where perfect absorption and interrogation of the plasmonic signal can be obtained. Through systematically optimizing the parameters of the transition metal dichalcogenide structured plasmonic substrate, we can balance the optical absorption efficiencies and the electron losses at the plasmonic resonance condition. All of the calculations were based on the transfer matrix method and Fresnel equations. A very low minimum reflectivity of $3.2560 \times 10^{-8}$ was demonstrated with an excitation wavelength of 1024 nm, showing a complete transfer (~100%) of the light energy into the plasmon resonance energy. The ultradark singularity at the resonance dip leads to an ultrahigh plasmonic sensitivity of $1.1 \times 10^{7}$ deg/RIU, which is 3 orders of magnitude higher than those with bare metallic sensing substrates used in commercial plasmonic sensors. The resolution is also improved by at least 3 orders of magnitude compared with conventional substrates.

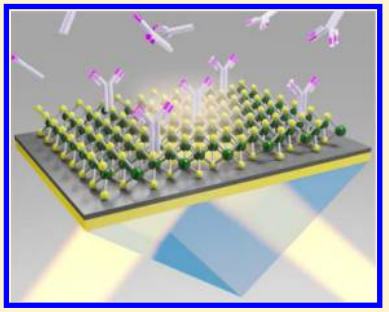

## INTRODUCTION

In past decades, surface plasmon resonance (SPR) based sensors have been widely studied and used in numerous biological and chemical applications, such as enzyme detection, medical diagnostics, and pharmaceutics.[1−8] SPR is known as the resonance of the incident photons and the surface plasmon polaritons (SPPs) at the interface between the negative and positive permittivity materials (e.g., metals and dielectrics). The resonance is sensitive to the perturbation of the surrounding media. Such a detection mechanism is suitable for label-free sensing and the real-time monitoring. However, the conventional SPR sensing approach is incapable of detecting small molecules with molecular weights less than 500 Da (e.g., hormone and drug molecules), especially at the picomolar concentration level ($1 \times 10^{-12}$ mol/L).[9] Recently, two-dimensional (2D) transition metal dichalcogenides (TMDCs) have attracted much attention from the scientific community and demonstrated their potential for improving the performances of various optoelectronic nanodevices such as photodetectors and solar cell elements.[10−14] The most intriguing optical property for them is the much higher absorption rate (~5%) than that of monolayer graphene (2.3%), with an atomic thickness less than 1 nm as well. Different from the zero band gap property of graphene, these 2D TMDCs exhibit a tunable band gap feature. The band gap can be tuned from indirect in their bulk forms to direct ones when their thickness was down to the monolayer scale. This makes them good candidates and complementary material to graphene for the future generation of integrated flexible electronic devices. The structures of these 2D TMDCs are also similar to that of graphene where the metal atom M (Mo, W) and the chalcogen atoms X (S, Se) are bonded in the form of X−M−X, with the

Received: December 22, 2016
Revised: February 24, 2017
Published: March 15, 2017






DOI: 10.1021/acs.jpcc.6b12858
J. Phys. Chem. C 2017, 121, 6282−6289

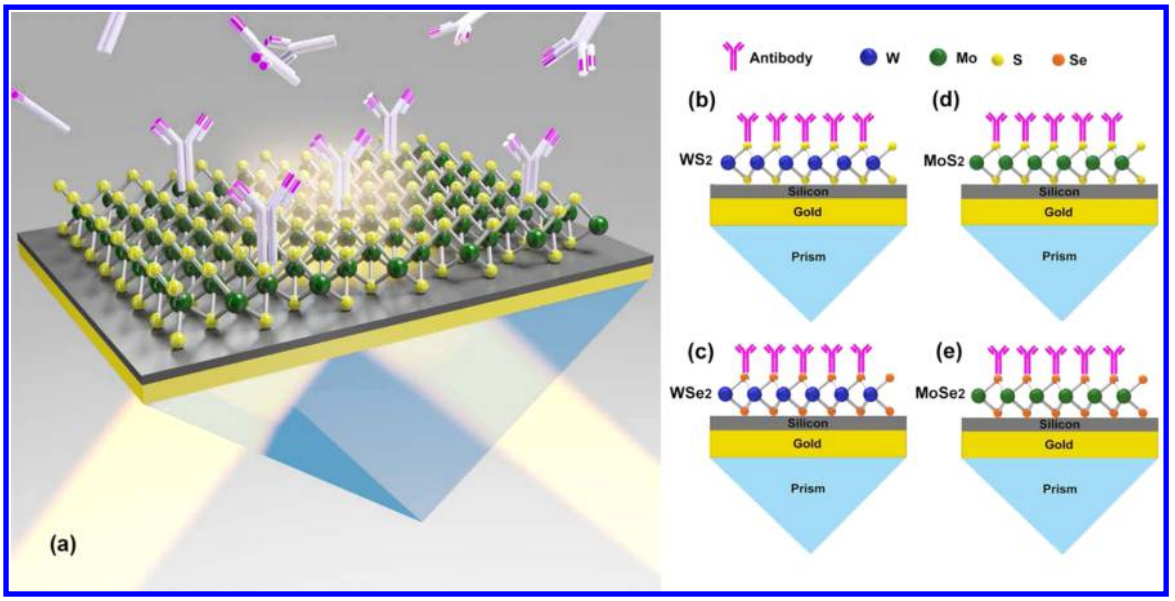


**Figure 1.** Schematic diagram of 2D TMDC structured on the plasmonic sensing substrate. (a) Antibody binding processes at the TMDC sensing surface that induced a tiny refractive index change ($1 \times 10^{-6}$ RIU). Atomically thin (b) $WS_2$, (c) $WSe_2$, (d) $MoS_2$, and (e) $MoSe_2$ layers structured at the sensing interface.

chalcogen atoms in two hexagonal planes separated by a plane of metal atoms. For the bulk TMDCs, they were stacked through van der Waals forces and thus a single layer can be easily obtained through an exfoliation process.[15−19] Currently, these atomic thin materials on a large area scale were synthesized by using the chemical vapor deposition (CVD) method. The multiple layers can also be fabricated by transferring the single layer and alternatively stacking onto the substrate. Previous literature has shown that structuring a thin layer of dielectric materials would change the plasmonic resonance condition, and also there are concerns drawn on the integration of the prism-coupling plasmonic sensors.[20,21] Engineering the plasmonic sensing substrate in a low cost and integrable way is highly desired for the commercial plasmonic sensor market. Here, we have systematically designed an optimized plasmonic sensing substrate with four TMDC materials ($MoS_2$, $WS_2$, $MoSe_2$, $WSe_2$) in terms of various excitation wavelengths from the visible to the near-infrared region. By tuning the number of TMDC layers and the thickness of gold/silicon thin films, a complete energy transfer from the incident light to the plasmon resonance energy was induced. This corresponds to a very low minimum reflectivity value at the resonance angle and a strong phase singularity that allows a large phase shift to a tiny refractive-index change of the sample solutions.

## METHODS

Schematic diagrams for the designed 2D TMDC structured on the plasmonic sensing substrate are shown in Figure 1. Since the surface plasmon resonance only affected the transverse magnetic (TM) waves, transverse electric (TE) waves here can be used as reference signals. In this way, the environmental noises can be effectively eliminated during the experimental progresses. To extract the phase signal changes from the reflected light, we use eq 1 to process the signals from TM (p-polarized) and TE (s-polarized) reflected light waves:

$$\varphi_d = |\varphi_p - \varphi_s| \tag{1}$$

**Table 1. Refractive Indexes and Thickness $T_{MX2}$ of Monolayer TMDCs in the Visible Region**

| TMDC | $T_{MX2}$ (nm) | $\lambda$ = 600 nm | $\lambda$ = 633 nm | $\lambda$ = 660 nm |
|---|---|---|---|---|
| $MoS_2$ | 0.65 | $n$ = 4.3934, $k$ = 1.2269 | $n$ = 5.0805, $k$ = 1.1723 | $n$ = 4.9991, $k$ = 1.2563 |
| $MoSe_2$ | 0.70 | $n$ = 4.7586, $k$ = 1.1504 | $n$ = 4.6226, $k$ = 1.0063 | $n$ = 4.4963, $k$ = 0.9382 |
| $WS_2$ | 0.80 | $n$ = 3.5202, $k$ = 0.6048 | $n$ = 4.8937, $k$ = 0.3124 | $n$ = 4.4735, $k$ = 0.2059 |
| $WSe_2$ | 0.70 | $n$ = 4.5039, $k$ = 0.9340 | $n$ = 4.5501, $k$ = 0.4332 | $n$ = 4.3357, $k$ = 0.2532 |

For the TM polarized (or p-polarized) light, the phase shift is dependent on the reflective coefficient $r_p$, as shown in eq 2, where $\theta_i$ and $\theta_t$ represent the incident angle and refracted angle respectively at the interface.

$$r_p = \frac{E_r}{E_i} = |r_p| e^{j\varphi} = \left| \frac{\tan(\theta_i - \theta_t)}{\tan(\theta_i + \theta_t)} \right| e^{j\varphi} \tag{2}$$

The phase of the TM polarized light is obtained as

$$\varphi_p = \arg(r_p) \tag{3}$$

The phase sensitivity $S$ is thus defined as the ratio of the change in differential phase $\Delta\varphi_d$ to the change in refractive index of the biomolecular sample layer $\Delta n_{bio}$, as follows:

$$S = \frac{\Delta\varphi_d}{\Delta n_{bio}} \tag{4}$$

where $\Delta\varphi_d$ indicates the differential phase change between TM and TE light waves.[5] The reflective coefficient $r_p$ is calculated by the Fresnel equation

$$r_p = \frac{E_{rp}}{E_{ip}} = \frac{n_t \cos\theta_i - n_i \cos\theta_t}{n_t \cos\theta_i + n_i \cos\theta_t} \tag{5}$$

and by Snell's law



DOI: 10.1021/acs.jpcc.6b12858
J. Phys. Chem. C 2017, 121, 6282−6289

Table 2. Refractive Indexes and Thickness $T_{MX2}$ of Monolayer TMDCs in the Near-Infrared Region

| TMDC | $\lambda$ = 785 nm | $\lambda$ = 904 nm | $\lambda$ = 1024 nm | $\lambda$ = 1150 nm | $\lambda$ = 1319 nm | $\lambda$ = 1540 nm |
|---|---|---|---|---|---|---|
| $MoS_2$ | $n$ = 4.6348, $k$ = 0.1163 | $n$ = 4.7261, $k$ = 0.1346 | $n$ = 4.8690, $k$ = 0.2444 | $n$ = 4.4317, $k$ = 0.0721 | $n$ = 4.3429, $k$ = 0.0433 | $n$ = 4.2374, $k$ = 0.0325 |
| $MoSe_2$ | $n$ = 4.2984, $k$ = 0.8225 | $n$ = 4.0212, $k$ = 0.4273 | $n$ = 3.8768, $k$ = 0.3561 | $n$ = 3.7965, $k$ = 0.2972 | $n$ = 3.6710, $k$ = 0.2343 | $n$ = 3.5281, $k$ = 0.1887 |
| $WS_2$ | $n$ = 4.0123, $k$ = 0.0399 | $n$ = 4.9916, $k$ = 0.2574 | $n$ = 4.5660, $k$ = 0.1058 | $n$ = 4.7071, $k$ = 0.1742 | $n$ = 4.5418, $k$ = 0.1688 | $n$ = 4.1715, $k$ = 0.1675 |
| $WSe_2$ | $n$ = 4.3655, $k$ = 0.0367 | $n$ = 5.1345, $k$ = 0.2692 | $n$ = 5.0110, $k$ = 0.2562 | $n$ = 4.9163, $k$ = 0.2234 | $n$ = 4.7083, $k$ = 0.1581 | $n$ = 4.4561, $k$ = 0.1496 |

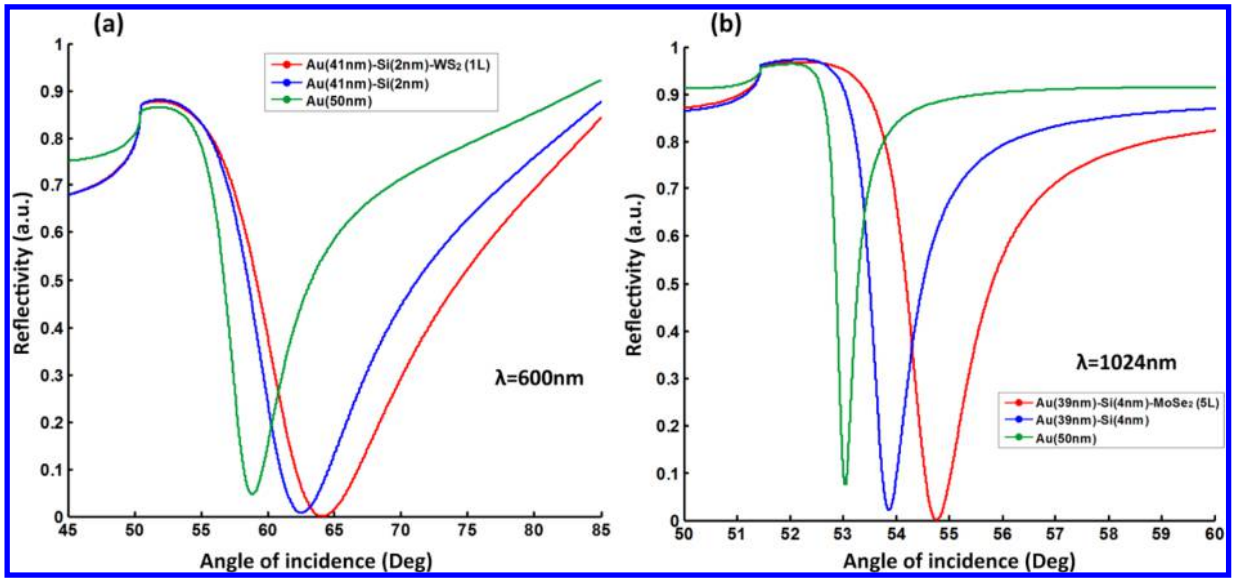


Figure 2. Plasmonic resonance curves showing that TMDC materials structured at the sensing surface could lead to a much lower minimum reflectivity and thus a complete energy transfer from the incident light to the plasmon resonance energy.

$$n_i \sin \theta_i = n_t \sin \theta_t \tag{6}$$

where $n_i$ and $n_t$ respectively represent the refractive indexes of the two media at the interface. The systematic reflective coefficient $r_p$ of the $N$-layered model should be calculated through the transfer matrix method (TMM). The matrix of the $N$-layer model can be defined as $M$, where $k$ represents the $k$th layer of the $N$-layered model.[22−24]

$$M = \prod_{k=2}^{N-1} M_k = \begin{bmatrix} M_{11} & M_{12} \\ M_{21} & M_{22} \end{bmatrix} \tag{7}$$

For the TM waves of the incident light, $M_k$ is given by

$$M_k = \begin{bmatrix} \cos \beta_k & -i \sin \beta_k / q_k \\ -i q_k \sin \beta_k & \cos \beta_k \end{bmatrix} \tag{8}$$

Here, the four elements $M_{11}$, $M_{12}$, $M_{21}$, and $M_{22}$ of the matrix $M$ can be obtained by given $q_k$ and $\beta_k$.

$$q_k = \frac{(\varepsilon_k - n_1^2 \sin^2 \theta_1)^{1/2}}{\varepsilon_k} = \frac{\lambda \beta_k}{2\pi d_k \varepsilon_k} \tag{9}$$

and

$$\beta_k = \frac{2\pi n_k \cos \theta_k (Z_k - Z_{k-1})}{\lambda} = \frac{2\pi d_k}{\lambda} (\varepsilon_k - n_1^2 \sin^2 \theta_1)^{1/2} \tag{10}$$

where $\theta_1$ is the incident angle at the first layer and $Z$ represent the boundary condition of the theoretical modeling. The first boundary of the tangential fields is defined as $Z_1 = 0$, and the last boundary $Z_{N-1}$ is given by

$$\begin{bmatrix} U_1 \\ V_1 \end{bmatrix} = M \begin{bmatrix} U_{N-1} \\ V_{N-1} \end{bmatrix} \tag{11}$$

where $U$ represents the tangential components of the electric fields at the interface, while $V$ denotes that in magnetic fields. Finally, the complex reflection coefficient, $r_p$, of the $N$-layer for the p-polarized light can be defined as

$$r_p = \frac{(M_{11} + M_{12} q_N) q_1 - (M_{21} + M_{22} q_N)}{(M_{11} + M_{12} q_N) q_1 + (M_{21} + M_{22} q_N)} \tag{12}$$

Thus, the corresponding reflectivity, $R_p$, can be obtained by the square of the reflection coefficient $r_p$:

$$R_p = |r_p|^2 \tag{13}$$

The full width at tenth maximum (FWTM) is investigated to characterize the detection accuracy of the SPR system; it is defined as the width of the SPR curve at the tenth of the maximum reflectivity $R_{FWTM}$:

$$R_{FWTM} = \frac{1}{10}(R_{max} + 9R_{min}) \tag{14}$$

where $R_{min}$ is the minimum reflectivity, whereas $R_{max}$ is the maximum reflectivity. The FWTM is the width of the SPR curve at the reflectivity that equals $R_{FWTM}$. According to eqs 9−12, the thickness and the refractive index (RI) of each layer are essential to obtain the reflectivity and phase. The wavelength-dependent refractive indexes of the six layers are given respectively as follows. The first layer of the N-layered model is the SF10 prism with the RI given by[25]



DOI: 10.1021/acs.jpcc.6b12858
J. Phys. Chem. C 2017, 121, 6282−6289

$$n_{\text{prism}}(\lambda) = \left( \frac{1.62153902\lambda^2}{\lambda^2 - 0.0122241457} + \frac{0.256287842\lambda^2}{\lambda^2 - 0.0595736775} + \frac{1.64447552\lambda^2}{\lambda^2 - 147.468793} \right)^{1/2} \quad (15)$$

where $\lambda$ denotes the excitation wavelength of the light source in micrometers (valid from 0.38 to 2.5 $\mu$m). The dispersion constants in the eq 15 were obtained from the data sheets provided by the optical glass product company Schott Inc. for N-SF10 prism. The complex refractive index of the second layer—gold thin film—was obtained from the experimental results of P. B. Johnson.[26] The refractive index of the third layer—silicon nanosheet—is determined by

$$n_{\text{silicon}}(\lambda) = A + A_1 e^{-\lambda/t_1} + A_2 e^{-\lambda/t_2} \quad (16)$$

with $A$ = 3.44904, $A_1$ = 2271.88813, $A_2$ = 3.39538, $t_1$ = 0.058304, and $t_2$ = 0.30384.[27] The $\lambda$ in eqs 15 and 16 represents the wavelength in micrometers. The absorption of the polycrystalline silicon nanolayers is very different from their bulk forms. It has been demonstrated that coating a thin layer of 10 nm polycrystalline silicon on the metallic substrate would not induce strong absorption in the visible region from 500 to 1000 nm.[28] The refractive indexes of the fourth layer—2D TMDC ($MoS_2$/$WS_2$/$MoSe_2$/$WSe_2$)—from the visible to the near-infrared range are provided in Tables 1 and 2[29,30] and Figure S1. The investigation of refractive index data for these novel 2D TMDC monolayers is an active research area. The complex refractive index used in the paper was obtained from two references based on the measurements from reflection spectra and spectroscopic ellipsometry.[29,30] According to current plasmonic literature studies, the dielectric constant of the 2D TMDC layers as isotropic materials is commonly assumed such as in refs 31−33. The complex refractive index $\bar{n}$ is defined as $\bar{n} = n + \kappa i$, where the real part $n$ indicates the phase velocity, while the imaginary part $\kappa$ known as the extinction coefficient refers to the mass attenuation coefficient.

## RESULTS AND DISCUSSION

Based on the transfer matrix method (TMM) and Fresnel equations mentioned above, we have systematically investigated the phase sensitivity with the 2D TMDC material structured SPR sensing substrates. It is worth noting that the phase sensitivity studied here is different from the traditional sensitivity through angular measurement. Since the phase change is dependent on the value of the minimum reflectivity in the SPR curve, it is more sensitive to the number of the 2D TMDC layers than the angular ones. The comparison details between the phase and angular interrogation are shown in Table S1 and Figure S2. The relationships between the reflectivity and the phase of different SPR substrates are shown in Table S2 and Figure 2. The substrate with the lower minimum reflectivity $R_{\text{min}}$ induces the larger changes in the differential phase, since the lowest $R_{\text{min}}$ indicates the largest energy transfer that corresponds to the strongest SPR electronic field. For the angular sensitivity enhancement, one usually needs to deposit more than 10 layers of atomically thin dielectric materials (e.g., graphene) on the metallic thin film for a pronounced improvement of the signal change. In this case, the resulting SPR curves were then of a much larger full width at half-maximum (FWHM) that corresponded to a lower detection accuracy. From Figure 2, we can see the comparison of SPR curves with bare Au thin film and the $WS_2$- or $MoSe_2$-structured sensing substrate. The coating of monolayer $WS_2$ and 5 layer $MoSe_2$ dielectric films led to a slight broadening of the resonance curves but a significantly lower minimum reflectivity. The increased width of the SPR curves was due to the electron damping energy loss that is related to the imaginary part of the dielectric constant of the 2D TMDC layers.[34,35] More importantly, the minimum reflectivity $R_{\text{min}}$ values for Au thin film of 50 nm (typical thickness of commercial SPR sensing slides) under the excitation wavelengths of 600 and 1024 nm are as large as 0.05 and 0.08 while the values for Si/$WS_2$ and Si/$MoSe_2$ are only 4.92 × $10^{-8}$ and 3.26 × $10^{-8}$. The lower $R_{\text{min}}$ values for 2D TMDC material structured sensing substrates indicated that the designed thin films had higher transfer efficiencies from the incident light to the plasmon resonance energy, leading to stronger SPR excitations and sharp phase jumps. Also, the resolutions of the 2D TMDC structured substrates are more than 2 orders of magnitude higher than those of the conventional ones, as shown in Table S3. However, further increase in the number of the 2D TMDC layers to a much thicker level would cause overabsorption of the incident light. Thus, there is a balance between the enhancement and absorption loss inside the 2D

**Table 3. Changes in Differential Phase, Minimum Reflectivity, and FWTM at the Optimum Au/Si Thickness with Different Numbers of TMDC layers, $\Delta n_{\text{bio}}$ = 1.2 × $10^{-4}$ RIU, and $\lambda_{\text{inc}}$ = 1024 nm**

| type of $MX_2$ | $d_{Si}$ (nm) | $d_{Au}$ (nm) | $MX_2$ (L) | $\Delta\varphi_d$ (deg) | $R_{\text{min}}$ | FWTM |
|---|---|---|---|---|---|---|
| $WS_2$ | 0 | 39 | 6 | 83.7199 | 4.57 × $10^{-7}$ | 0.4777 |
| $WS_2$ | 1 | 42 | 1 | 62.9637 | 1.15 × $10^{-5}$ | 0.2357 |
| $WS_2$ | 2 | 40 | 4 | 68.0817 | 4.03 × $10^{-6}$ | 0.4163 |
| $WS_2$ | 3 | 40 | 4 | 87.5683 | 3.91 × $10^{-7}$ | 0.4546 |
| $WS_2$ | 4 | 42 | 1 | 57.9695 | 1.53 × $10^{-5}$ | 0.2970 |
| $WS_2$ | 5 | 43 | 0 | 69.1099 | 6.28 × $10^{-6}$ | 0.2663 |
| $WS_2$ | 6 | 43 | 0 | 79.2962 | 4.34 × $10^{-7}$ | 0.2874 |
| $WS_2$ | 7 | 43 | 0 | 76.2760 | 1.82 × $10^{-6}$ | 0.3104 |
| $MoSe_2$ | 0 | 42 | 1 | 91.8140 | 1.74 × $10^{-7}$ | 0.2117 |
| $MoSe_2$ | 1 | 42 | 1 | 86.8287 | 2.65 × $10^{-7}$ | 0.2279 |
| $MoSe_2$ | 2 | 42 | 1 | 78.2922 | 5.00 × $10^{-7}$ | 0.2456 |
| $MoSe_2$ | 3 | 42 | 1 | 84.0054 | 9.90 × $10^{-7}$ | 0.2648 |
| $MoSe_2$ | 4 | 39 | 5 | 106.9330 | 3.26 × $10^{-8}$ | 0.4853 |
| $MoSe_2$ | 5 | 42 | 1 | 74.2272 | 3.75 × $10^{-6}$ | 0.3088 |
| $MoSe_2$ | 6 | 43 | 0 | 79.2962 | 4.34 × $10^{-7}$ | 0.2874 |
| $MoSe_2$ | 7 | 43 | 0 | 76.2760 | 1.82 × $10^{-6}$ | 0.3104 |
| $MoS_2$ | 0 | 42 | 4 | 69.2605 | 4.44 × $10^{-6}$ | 0.2623 |
| $MoS_2$ | 1 | 42 | 4 | 71.7154 | 4.61 × $10^{-6}$ | 0.2839 |
| $MoS_2$ | 2 | 42 | 4 | 70.9399 | 4.24 × $10^{-6}$ | 0.3074 |
| $MoS_2$ | 3 | 42 | 4 | 70.5056 | 3.37 × $10^{-6}$ | 0.3332 |
| $MoS_2$ | 4 | 42 | 4 | 75.1060 | 2.09 × $10^{-6}$ | 0.3618 |
| $MoS_2$ | 5 | 42 | 4 | 76.0397 | 7.74 × $10^{-7}$ | 0.3932 |
| $MoS_2$ | 6 | 43 | 0 | 79.2962 | 4.34 × $10^{-7}$ | 0.2874 |
| $MoS_2$ | 7 | 42 | 4 | 82.6321 | 8.40 × $10^{-7}$ | 0.4669 |
| $WSe_2$ | 0 | 41 | 3 | 44.9583 | 3.52 × $10^{-5}$ | 0.2763 |
| $WSe_2$ | 1 | 40 | 5 | 65.5617 | 5.20 × $10^{-6}$ | 0.3904 |
| $WSe_2$ | 2 | 40 | 5 | 87.9733 | 2.66 × $10^{-7}$ | 0.4259 |
| $WSe_2$ | 3 | 41 | 3 | 71.5747 | 2.45 × $10^{-6}$ | 0.3524 |
| $WSe_2$ | 4 | 41 | 3 | 79.6861 | 1.53 × $10^{-7}$ | 0.3829 |
| $WSe_2$ | 5 | 41 | 3 | 80.5496 | 3.66 × $10^{-7}$ | 0.4167 |
| $WSe_2$ | 6 | 43 | 0 | 79.2962 | 4.34 × $10^{-7}$ | 0.2874 |
| $WSe_2$ | 7 | 43 | 0 | 76.2760 | 1.82 × $10^{-6}$ | 0.3104 |



DOI: 10.1021/acs.jpcc.6b12858
J. Phys. Chem. C 2017, 121, 6282−6289

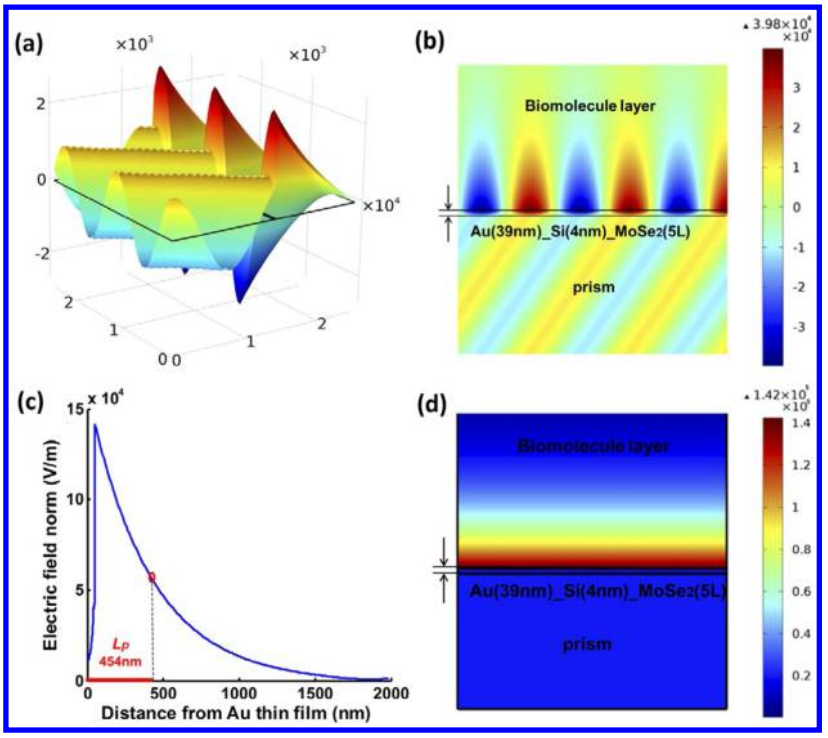


**Figure 3.** Finite element analyses (FEA) showing the electric field distribution of 2D TMDC structured substrate under the resonance condition ($\lambda_{inc}$ = 1024 nm). (a) The *y* components of the electric field distribution shown in 3D space. (b) The *y* components of the electric field distribution shown in 2D interface. (a) and (b) share the same color bar. (c) Evanescent decay of the excited electric field penetrating into the sample medium. The red line indicates the penetration depth $L_p$ of ∼454 nm. (d) Distribution of the electric field norm.

TMDC structured metallic thin films during our optimization processes.

To test the performances of the engineered 2D TMDC phase-sensitive SPR sensors, we have assumed a refractive-index change to the sample layers ($\Delta n_{bio}$ = 0.00012 RIU; RIU here is short for refractive-index unit) that corresponds to standard single stranded DNA binding interactions with a low concentration in a picomolar range. As shown in Table 3, Tables S4−S11, and Figures S3 and S4, parameters including the number of TMDC layers, silicon/gold thickness, and excitation wavelength were considered and tuned to obtain the largest phase signal change and narrow curve width. It is shown in the table results that the largest phase signal change ($\Delta\varphi_d$) always corresponded to the lowest minimum reflectivity ($R_{min}$). This phenomenon is consistent for all four types of 2D TMDC layers with different excitation wavelengths ranging from the visible to the near-infrared region (600−1540 nm). Moreover, the curve widths increased significantly with the number of the TMDC layers due to their overabsorption for a fixed excitation wavelength. Thus, we cannot select the one with a larger number of TMDC layers as the optimum configuration; even a low $R_{min}$ could be obtained. For a general case even without TMDC layers, the curve widths were much narrower under the excitation wavelengths in the near-infrared region than those in the visible region. This is attributed to the fact that the real part of the Au dielectric constant is increased more significantly than the imaginary part in the longer excitation wavelength that led to a low electron damping loss in the metallic layer. Here, we need to consider another important parameter: the penetration depth of the surface plasmon resonance. As the excited surface plasmon waves exponentially decay from the sensing interface as shown in Figure 3, the penetration depth ($L_p$) was defined as the resonance depth where the excited electric field decreased by a factor 1/e.[4] The value of the penetration depth ($L_p$) is known to be increased sharply with the excitation wavelength. The longer penetration depth would make the excited surface plasmon waves more sensitive to the refractive index changes that were relatively far from the sensing interface and would increase the noise level of the signals during the experimental measurements. The detailed study on the evanescent field and the penetration depth is shown in Figure S5 and Table S12. Based on the above discussions, we selected four optimum configuration of the 2D TMDC structured sensing substrates for different excitation wavelengths (i.e., monolayer $WS_2$ structured on 41 nm of Au under 600 nm, 6-layer $MoS_2$ structured on 47 nm of Au under 785 nm, bilayer $WSe_2$ structured on 45 nm of Au under 904 nm, and 5-layer $MoSe_2$ structured on 39 nm of Au under 1024 nm).

In Figure 4, we have plotted the differential phase changes in terms of a large refractive-index change ($\Delta n_{bio}$) from 0 to 0.0015 RIU by using these selected 2D TMDC structured sensing substrates. The phase signals for the optimum number of TMDC layers showed a much sharper change in comparison to those with the nonoptimum ones, and more details were shown in Tables S2 and S13. The significant difference in the phase signal change ($\Delta\varphi_d$) is due to the large difference in the minimum reflectivity ($R_{min}$) induced by the TMDC layers under the plasmon resonance condition as listed in Table 3 and Table S2. As discussed above, further increase in the number of 2D TMDC layers to a much thicker level would cause the overabsorption of the incident light. Among these four optimized 2D TMDC structured sensing configurations, 5-layer $MoSe_2$ structured on 39 nm of Au under 1024 nm exhibited the lowest minimum reflectivity of $3.2560 \times 10^{-8}$ and therefore the highest phase sensitivity of $1.128395 \times 10^{7}$ deg/RIU. The comparisons of the sensing performances for


DOI: 10.1021/acs.jpcc.6b12858
J. Phys. Chem. C 2017, 121, 6282−6289

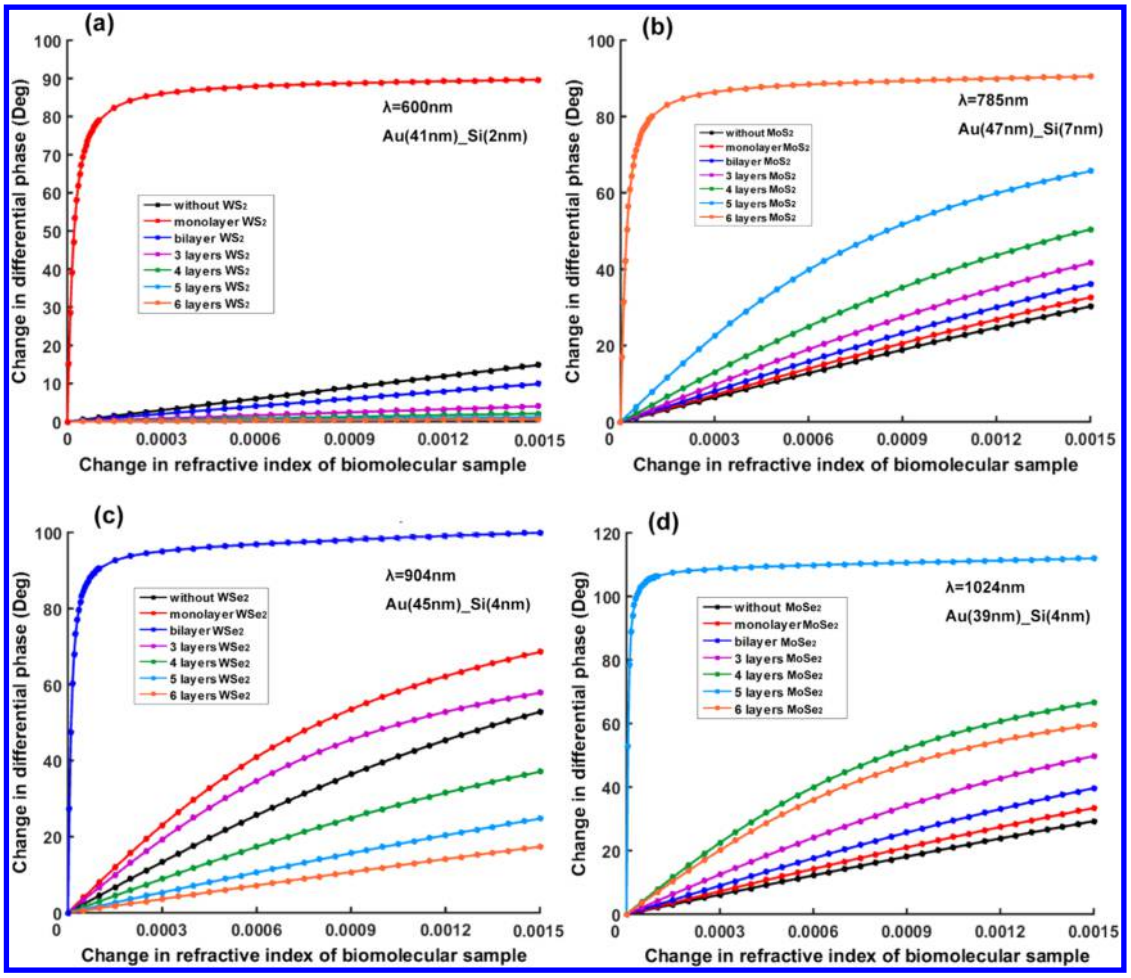


**Figure 4.** Optimization of the number of TMDC layers in terms of the differential phase shift $\Delta\varphi_d$ to the refractive index change of sample solutions $\Delta n_{bio}$. The excitation wavelength $\lambda_{inc}$ was fixed at optimum wavelength selected from Table 3 and Tables S4–S11.

**Table 4. Comparison of Plasmonic Sensing Performances with or without Optimum Selected TMDC Layers Structured on Au Substrate ($\Delta n_{bio} = 2 \times 10^{-6}$)[a]**

| enhanced model | resonance angle (deg) | min reflectivity | FWTM (deg) | $\Delta\varphi_d$ (deg) | sensitivity (deg/RIU) |
|---|---|---|---|---|---|
| Au (39 nm)/Si (4 nm)/$MoSe_2$ (5 L) | 54.7660 | $3.2560 \times 10^{-8}$ | 0.4853 | 22.5679 | $1.128395 \times 10^7$ |
| Au (39 nm)/Si (4 nm) | 53.8679 | 0.0217 | 0.3109 | 0.0409 | $2.043310 \times 10^4$ |
| Au (50 nm) | 53.0390 | 0.0742 | 0.1353 | 0.0255 | $1.275259 \times 10^4$ |

[a]High phase sensitivities always correspond to low minimum reflectivity, showing the TMDC layers have induced a strong phase singularity.

plasmonic substrates with or without the 5-layer $MoSe_2$ have been listed in Table 4. The phase sensitivity of $1.128395 \times 10^7$ deg/RIU with our designed 2D TMDC structured sensing substrates is demonstrated to be 3 orders of magnitude higher than that with the conventional Au thin film with 50 nm thickness—$1.275259 \times 10^4$ deg/RIU—showing a much more improved sensing performance for a tiny refractive index change ($2 \times 10^{-6}$ RIU), and thus would be more sensitive to small molecular interactions at the sensing interface.

The graphic comparison between the TMDC enhanced substrates and the conventional ones is shown in Figure S6. In addition, the phase changes of the TMDC based structures are much higher than those of the graphene and the hexagonal boron nitride (hBN) based ones. Although graphene and hBN have been explored as excellent 2D materials in photoelectric applications,[36,37] they have less potential than TMDCs in the SPR sensing field due to the relatively low refractive index. The details are shown in Figures S7–S11 and Table S14.

## CONCLUSION

In this work, we have designed atomically thin 2D TMDC structured plasmonic sensing substrates for the enhancement of the SPR phase detection sensitivity. To make the structures more compatible and cost-effective for future miniaturization as integrated optoelectronic devices, a thin layer of silicon was engineered at the sensing interface as well. The high optical absorption rate of the TMDC layer and precise tuning of the layer thickness in a step less than 1 nm allows the achievement of the ultralow minimum reflectivity up to $3.2560 \times 10^{-8}$ at the resonance angle. It is known that the low minimum reflectivity at the plasmonic resonance condition would lead to the singularity of the phase signals. The phase singularity makes the signal very sensitive to the refractive-index change of the sample solutions at the sensing interface. This is mainly due to two reasons: (i) The reflected p-polarized light experiences a jumplike phase shift when the SPR effect is excited. This allows


DOI: 10.1021/acs.jpcc.6b12858
J. Phys. Chem. C 2017, 121, 6282–6289

orders of magnitude higher signal changes than other sensing parameters, e.g. intensity and resonance angle. (ii) The SPR phase signal is extracted from the differential phase between p-polarized and s-polarized light. This action removes the environmental noise and improves the signal-to-noise ratio, since the s-polarized light here is used as a reference. Moreover, the deeper resonance depth in the plasmonic curves also indicated a complete energy transfer from the incident light into the plasmon resonance. Since there is a balance between the absorption enhancement effect and absorption loss induced by the extra electron damping related to the imaginary part of the dielectric constant of TMDC layers, we have systematically optimized various parameters for the 2D TMDC structured plasmonic sensing configurations such as the Au and Si thicknesses, the number of TMDC layers, and the excitation wavelengths. The highest phase sensitivity of $1.1 \times 10^7$ deg/RIU was achieved with 5-layer $MoSe_2$ structured on 39 nm of Au under an excitation wavelength of 1024 nm, which is 3 orders of magnitude higher than that of $1.3 \times 10^4$ deg/RIU with bare Au thin film with 50 nm thickness used in commercial plasmonic sensors.

## ■ ASSOCIATED CONTENT

### Supporting Information

The Supporting Information is available free of charge on the ACS Publications website at DOI: 10.1021/acs.jpcc.6b12858.

Sensitivity comparison between phase and angular interrogation; resolution of four types of TMDC enhanced structures; SPR enhancement comparison among 2D TMDCs, graphene, and hBN; detailed penetration depth of four types of TMDC enhanced structures; detailed phase change, minimum reflectivity, and curve width for TMDC substrates under excitation wavelengths from 600 to 1540 nm; detail of sensing parameters and electric field of optimized TMDC enhanced substrate at visible excitation wavelength; phase sensitivity for tiny refractive index change in sample of $10^{-5}$ RIU; graphic refractive index of TMDCs (PDF)

## ■ AUTHOR INFORMATION


### Corresponding Authors

*E-mail: jlqu@szu.edu.cn. Tel.: 86-0755-26538580.
*E-mail: ktyong@ntu.edu.sg. Tel.: 65-67905444.

### ORCID

Qingling Ouyang: 0000-0002-5483-1315
Shuwen Zeng: 0000-0003-2188-7213
Ken-Tye Yong: 0000-0001-7936-2941

### Author Contributions

▽Q.O. and S.Z.: These authors contributed equally to this work.


### Notes

The authors declare no competing financial interest.

## ■ ACKNOWLEDGMENTS

This work was supported by the Singapore Ministry of Education (Grants Tier 2 MOE2010-T2-2-010 (M4020020.040 ARC2/11) and Tier 1 M4010360.040 RG29/10), NTU–NHG Innovation Collaboration Grant (No. M4061202.040), A*STAR Science and Engineering Research Council (No. M4070176.040), and School of Electrical and Electronic Engineering at NTU.

## ■ REFERENCES


(1) Zeng, S.; Yong, K.-T.; Roy, I.; Dinh, X.-Q.; Yu, X.; Luan, F. A Review on Functionalized Gold Nanoparticles for Biosensing Applications. *Plasmonics* **2011**, *6*, 491–506.
(2) Zeng, S.; Baillargeat, D.; Ho, H. P.; Yong, K.-T. Nanomaterials Enhanced Surface Plasmon Resonance for Biological and Chemical Sensing Applications. *Chem. Soc. Rev.* **2014**, *43*, 3426–3452.
(3) Huang, Y. H.; Ho, H. P.; Kong, S. K.; Kabashin, A. V. Phase-sensitive Surface Plasmon Resonance Biosensors: Methodology, Instrumentation and Applications. *Ann. Phys.* **2012**, *524*, 637–662.
(4) Homola, J.; Piliarik, M. Surface Plasmon Resonance (SPR) Sensors. In *Surface Plasmon Resonance Based Sensors*; Springer: 2006; pp 45–67.
(5) Shalabney, A.; Abdulhalim, I. Sensitivity-enhancement Methods for Surface Plasmon Sensors. *Laser Photon. Rev.* **2011**, *5*, 571–606.
(6) Fang, Y.; Phillips, B. M.; Askar, K.; Choi, B.; Jiang, P.; Jiang, B. Scalable Bottom-up Fabrication of Colloidal Photonic Crystals and Periodic Plasmonic Nanostructures. *J. Mater. Chem. C* **2013**, *1*, 6031–6047.
(7) Fang, Y.; Ni, Y.; Choi, B.; Leo, S.-Y.; Gao, J.; Ge, B.; Taylor, C.; Basile, V.; Jiang, P. Chromogenic Photonic Crystals Enabled by Novel Vapor-Responsive Shape-Memory Polymers. *Adv. Mater.* **2015**, *27*, 3696–3704.
(8) Fang, Y.; Ni, Y.; Leo, S.-Y.; Taylor, C.; Basile, V.; Jiang, P. Reconfigurable Photonic Crystals enabled by Pressure-Responsive Shape-memory Polymers. *Nat. Commun.* **2015**, *6*, 7416.
(9) Kabashin, A. V.; Evans, P.; Pastkovsky, S.; Hendren, W.; Wurtz, G. A.; Atkinson, R.; Pollard, R.; Podolskiy, V. A.; Zayats, A. V. Plasmonic Nanorod Metamaterials for Biosensing. *Nat. Mater.* **2009**, *8*, 867–871.
(10) Lu, X.; Utama, M. I. B.; Lin, J. H.; Gong, X.; Zhang, J.; Zhao, Y. Y.; Pantelides, S. T.; Wang, J. X.; Dong, Z. L.; Liu, Z.; et al. Large-Area Synthesis of Monolayer and Few-Layer $MoSe_2$ Films on $SiO_2$ Substrates. *Nano Lett.* **2014**, *14*, 2419–2425.
(11) Jariwala, D.; Sangwan, V. K.; Lauhon, L. J.; Marks, T. J.; Hersam, M. C. Emerging Device Applications for Semiconducting Two-Dimensional Transition Metal Dichalcogenides. *ACS Nano* **2014**, *8*, 1102–1120.
(12) Huang, X.; Zeng, Z. Y.; Zhang, H. Metal Dichalcogenide Nanosheets: Preparation, Properties and Applications. *Chem. Soc. Rev.* **2013**, *42*, 1934–1946.
(13) Wang, Q. H.; Kalantar-Zadeh, K.; Kis, A.; Coleman, J. N.; Strano, M. S. Electronics and Optoelectronics of Two-Dimensional Transition Metal Dichalcogenides. *Nat. Nanotechnol.* **2012**, *7*, 699–712.
(14) Kuc, A.; Zibouche, N.; Heine, T. Influence of Quantum Confinement on the Electronic Structure of the Transition Metal Sulfide $TS_2$. *Phys. Rev. B: Condens. Matter Mater. Phys.* **2011**, *83*, 245213.
(15) Pospischil, A.; Furchi, M. M.; Mueller, T. Solar-energy Conversion and Light Emission in an Atomic Monolayer p-n Diode. *Nat. Nanotechnol.* **2014**, *9*, 257–261.
(16) Britnell, L.; Ribeiro, R. M.; Eckmann, A.; Jalil, R.; Belle, B. D.; Mishchenko, A.; Kim, Y. J.; Gorbachev, R. V.; Georgiou, T.; Morozov, S. V.; et al. Strong Light-Matter Interactions in Heterostructures of Atomically Thin Films. *Science* **2013**, *340*, 1311–1314.
(17) Tsai, M. L.; Su, S. H.; Chang, J. K.; Tsai, D. S.; Chen, C. H.; Wu, C. I.; Li, L. J.; Chen, L. J.; He, J. H. Monolayer $MoS_2$ Heterojunction Solar Cells. *ACS Nano* **2014**, *8*, 8317–8322.
(18) Atwater, H. A.; Polman, A. Plasmonics for Improved Photovoltaic Devices. *Nat. Mater.* **2010**, *9*, 205–213.
(19) Giovannetti, G.; Khomyakov, P. A.; Brocks, G.; Karpan, V. M.; van den Brink, J.; Kelly, P. J. Doping Graphene with Metal Contacts. *Phys. Rev. Lett.* **2008**, *101*, 026803.




DOI: 10.1021/acs.jpcc.6b12858
J. Phys. Chem. C 2017, 121, 6282–6289

(20) Le, K. Q.; Ngo, Q. M. A Silicon-on-insulator Surface Plasmon Interferometer for Hydrogen Detection. *J. Appl. Phys.* **2016**, *120*, 043106.
(21) Le, K. Q.; Bienstman, P. Enhanced Sensitivity of Silicon-on-insulator Surface Plasmon Interferometer with Additional Silicon Layer. *IEEE Photonics J.* **2011**, *3*, 538−545.
(22) Homola, J.; Koudela, I.; Yee, S. S. Surface Plasmon Resonance Sensors based on Diffraction Gratings and Prism Couplers: Sensitivity Comparison. *Sens. Actuators, B* **1999**, *54*, 16−24.
(23) Wu, S. Y.; Ho, H. P.; Law, W. C.; Lin, C. L.; Kong, S. K. Highly Sensitive Differential Phase-sensitive Surface Plasmon Resonance Biosensor Based on the Mach-Zehnder Configuration. *Opt. Lett.* **2004**, *29*, 2378−2380.
(24) Schasfoort, R. B.; Tudos, A. J.: *Handbook of Surface Plasmon Resonance*; Royal Society of Chemistry: 2008.
(25) Polyanskiy, M. N. Refractive Index Database. Available at http://refractiveindex.info (accessed Feb 20, 2016).
(26) Johnson, P. B.; Christy, R.-W. Optical Constants of the Noble Metals. *Phys. Rev. B* **1972**, *6*, 4370−4379.
(27) Palik, E. D. *Handbook of Optical Constants of Solids*; Academic Press: 1998; Vol. 3.
(28) Mirshafieyan, S. S.; Guo, J. Silicon Colors: Spectral Selective Perfect Light Absorption in Single Layer Silicon Films on Aluminum Surface and its Thermal Tunability. *Opt. Express* **2014**, *22*, 31545−31554.
(29) Li, Y. L.; Chernikov, A.; Zhang, X.; Rigosi, A.; Hill, H. M.; van der Zande, A. M.; Chenet, D. A.; Shih, E. M.; Hone, J.; Heinz, T. F. Measurement of the Optical Dielectric Function of Monolayer Transition-Metal Dichalcogenides: $MoS_2$, $MoSe_2$, $WS_2$, and $WSe_2$. *Phys. Rev. B: Condens. Matter Mater. Phys.* **2014**, *90*, 205422.
(30) Liu, H. L.; Shen, C. C.; Su, S. H.; Hsu, C. L.; Li, M. Y.; Li, L. J. Optical Properties of Monolayer Transition Metal Dichalcogenides Probed by Spectroscopic Ellipsometry. *Appl. Phys. Lett.* **2014**, *105*, 201905.
(31) Bahauddin, S. M.; Robatjazi, H.; Thomann, I. Broadband Absorption Engineering to Enhance Light Absorption in Monolayer $MoS_2$. *ACS Photonics* **2016**, *3*, 853−862.
(32) Mishra, A. K.; Mishra, S. K.; Verma, R. K. Graphene and Beyond Graphene $MoS_2$: A New Window in Surface-Plasmon-Resonance-Based Fiber Optic Sensing. *J. Phys. Chem. C* **2016**, *120*, 2893−2900.
(33) Lin, Z.; Jiang, L.; Wu, L.; Guo, J.; Dai, X.; Xiang, Y.; Fan, D. Tuning and Sensitivity Enhancement of Surface Plasmon Resonance Biosensor with Graphene Covered Au-$MoS_2$-Au Films. *IEEE Photonics J.* **2016**, *8*, 4803308.
(34) Pockrand, I. Surface Plasma-Oscillations at Silver Surfaces with Thin Transparent and Absorbing Coatings. *Surf. Sci.* **1978**, *72*, 577−588.
(35) Pockrand, I.; Swalen, J. D.; Gordon, J. G.; Philpott, M. R. Surface-Plasmon Spectroscopy of Organic Monolayer Assemblies. *Surf. Sci.* **1978**, *74*, 237−244.
(36) Dai, S.; Ma, Q.; Liu, M. K.; Andersen, T.; Fei, Z.; Goldflam, M. D.; Wagner, M.; Watanabe, K.; Taniguchi, T.; Thiemens, M.; et al. Graphene on hexagonal boron nitride as a tunable hyperbolic metamaterial. *Nat. Nanotechnol.* **2015**, *10*, 682−686.
(37) Rivero, P.; Horvath, C. M.; Zhu, Z.; Guan, J.; Tománek, D.; Barraza-Lopez, S. Simulated Scanning Tunneling Microscopy Images of Few-layer Phosphorus Capped by Graphene and Hexagonal Boron Nitride Monolayers. *Phys. Rev. B: Condens. Matter Mater. Phys.* **2015**, *91*, 115413.


DOI: 10.1021/acs.jpcc.6b12858
*J. Phys. Chem. C* 2017, 121, 6282−6289